Acta Crystallographica Section A
Foundations of Crystallography
ISSN 0108-7673

Received 24 February 2005
Accepted 26 April 2005

Electron-density distribution in cubic $SrTiO_3$: a comparative γ-ray diffraction study

W. Jauch[a]* and M. Reehuis[b]

[a]Hahn-Meitner-Institut, Glienicker Strasse 100, D-14109 Berlin, Germany, and [b]Max-Planck-Institut für Festkörperforschung, Heisenbergstrasse 1, D-70569 Stuttgart, Germany. Correspondence e-mail: jauch@hmi.de

The electron density and atomic displacements in the perovskite $SrTiO_3$ have been studied using extensive and accurate γ-ray diffraction data ($\lambda = 0.0392$ Å) at room temperature. The six strongest low-order structure factors have been determined under extinction-free conditions. Gram–Charlier series expansion of the thermal parameters have revealed no evidence for anharmonicity. The population of the 3*d* subshell on Ti is found to be close to zero, in agreement with the observed magnetic behaviour. The electronic properties at the bond critical points indicate ionic Ti—O and Sr—O interactions of different strengths, which is corroborated by the net charges of the atomic basins [q(Sr) = 1.18 |e|, q(Ti) = 3.10 |e|, q(O) = −1.42 |e|]. A critical comparison is made with earlier experimental results from laboratory X-ray, synchrotron X-ray, electron and neutron diffraction studies. Agreement and discrepancies are identified and resolved.

1. Introduction

The prototype perovskite $SrTiO_3$ is one of the most thoroughly studied materials in solid-state physics owing to a variety of unusual properties, in particular dielectric ones. It is an incipient ferroelectric that remains cubic down to $T_c \approx 106$ K, where it undergoes an antiferrodistortive phase transition with cell doubling. The paraelectric phase is stabilized by the large zero-point motion of Ti (Jauch & Palmer, 1999) but small perturbations such as electric fields, elastic strains or impurities can destroy the stability and induce a ferroelectric phase. Though the many departures from the basic cubic structure in the perovskite series are of fundamental interest, further insight into their nature should be obtained by a thorough exploration of the ideal case.

The experimental determination of the charge density in cubic $SrTiO_3$ has been the object of several publications. Two back-to-back papers appeared in 1995, reporting studies employing synchrotron (Maslen *et al.*, 1995) and laboratory X-rays (Abramov *et al.*, 1995). The basis of both papers was examination of dynamic Fourier deformation maps. The results were contradictory and, as urged by Spackman (1998): 'It seems important to the future of the field that the source of substantial disagreements between the outcomes of similar studies such as these be clearly identified and widely published'. The disagreement applies not only to the charge density but to the atomic probability density functions as well. X-ray studies of inorganic materials with heavier atoms have an inherent loss of accuracy since they are prone to be affected by systematic errors introduced in the process of deriving structure factors from the observed intensities, such as extinction, absorption and dispersion corrections. Some of the problems are removed by convergent-beam electron diffraction which can provide extinction-free low-order structure factors on an absolute scale. By complementing such measurements with conventional higher-order X-ray diffraction data, the charge density is accessible. One must be aware, however, that its reliability depends crucially on the quality of the X-ray data set. This method has recently been applied to $SrTiO_3$ (Friis *et al.*, 2004) using the X-ray data from Abramov *et al.* (1995), which in turn have been reanalysed by Zhurova & Tsirelson (2002) in terms of a multipole model.

In this work, we present a complete high-accuracy charge-density analysis of cubic $SrTiO_3$ using 316.5 keV γ radiation. It is part of a continuing study of the real-space electronic structure of archetype inorganic crystals of relatively simple structure. The benefits from the use of high-quality γ-ray structure factors in such studies have been exploited and demonstrated in a series of experiments during the past decade (*e.g.* Jauch, 2004). A detailed comparative assessment of agreement and disagreement will be given with earlier results on $SrTiO_3$, as deduced from laboratory X-ray, synchrotron X-ray, electron and neutron diffraction work. The charge-density issues centre around the role of the 3*d* electrons as well as the relative ionic and covalent bonding contributions.

2. Experimental and data treatment

At room temperature, $SrTiO_3$ has the ideal perovskite structure (space group $Pm\bar{3}m$, $Z = 1$) with Sr at 1*a* (0,0,0), Ti at

1*b* ($\frac{1}{2},\frac{1}{2},\frac{1}{2}$), and O at 3*c* ($\frac{1}{2},\frac{1}{2},0$). The lattice constant is $a = 3.905$ Å at 293 K (Okazaki & Kawaminami, 1973).

The single crystal used in the present investigation was a Verneuil-grown cuboid of dimensions 3.32 × 3.26 × 3.19 mm, purchased from Lamprecht/Neuhausen (Germany). The same sample has been used in previous γ-ray work devoted to the analysis of thermal motion above and below the cubic-to-tetragonal phase transition at $T_c \approx 106$ K (Jauch & Palmer, 1999). High-resolution double-crystal rocking curves, using a perfect Si crystal as collimator, had full widths at half-maximum (FWHM) varying between 40 and 60 arc s for different crystal directions. X-ray fluorescence analysis by means of synchrotron radiation was applied to check for the presence of Ba or Ca impurities in the sample. The content of these elements was found to be lower than 200 parts in 10^6.

Bragg intensities have been measured under ambient conditions on the γ-ray diffractometer installed at the Hahn-Meitner-Institut, where the most intense line of an ^{192}Ir source ($T_{1/2} = 73.83$ d) with a wavelength of 0.0392 Å (316.5 keV) is used. The diffracted γ rays were recorded in ω-step-scan mode with an intrinsic germanium detector. 776 integrated intensities were collected, corresponding to 174 independent reflections with a precision factor of $\sum\sigma(I)/\sum I = 0.82\%$. The data set extends to $\sin\theta/\lambda = 1.72$ Å^{-1}, with a completeness of 63% at the 1.6 Å^{-1} limit.

The six strongest low-order reflections were measured in transmission geometry from a platelet with edges 15 mm ∥ [001], 5 mm ∥ [110] and 0.3 mm ∥ [$\bar{1}$10], thus providing extinction-free structure factors. The intensities from the platelet were calibrated to absolute scale by means of the (200) intensity from an ideally imperfect Si crystal. The mean statistical precision of these particular data, $\sigma(I)/I = 0.9\%$, was dominated by the uncertainty in the scaling.

An absorption correction was carried out [$\mu = 0.507$ cm^{-1} (Hubbel, 1982)] using the *Xtal* (Hall *et al.*, 1995) program suite, resulting in a transmission range from 0.846 to 0.859. The data were corrected for the contribution of inelastic thermal diffuse scattering (TDS) to the total intensity. The formalism of Skelton & Katz (1969) was applied, using the elastic constants from Bell & Rupprecht (1963) and the instrumental parameters defining the sampled volume in reciprocal space. The maximum TDS contribution was only 3% for the highest-order reflection.[1]

3. Charge-density refinement

Least-squares refinements were performed with the program *VALRAY* (Stewart *et al.*, 2000), minimizing $\chi^2 = \sum w(|F_o|^2 - |F_c|^2)^2$, where F_o and F_c are the observed and calculated structure factors, respectively. The weights of the data points, $w = 1/\sigma^2(F_o^2)$, were based solely on the counting-statistical variances (except for the six low-order reflections with an additional contribution from scaling uncertainty).

[1] Supplementary data for this paper are available from the IUCr electronic archives (Reference: SH5025). Services for accessing these data are described at the back of the journal.

Table 1
Quality of fit for the various scattering models; *Np* = number of adjustable parameters; number of observations = 776 (174 unique data).

The scale factor was fixed to the value obtained from a high-order IAM refinement ($\sin\theta/\lambda \geq 0.7$ Å^{-1}).

	IAM	Monopoles	Multipoles
χ^2	5365.6	1646.8	1505.2
Np	5	8	13

The extinction length for the strongest reflection amounts to 100 μm, so that the presence of primary extinction can be ruled out. Secondary extinction was treated according to the Becker & Coppens (1975) formalism by refining the width parameter of a Gaussian mosaic distribution. The different absorption-weighted path lengths through the crystal varied by 10% and symmetry-equivalent reflections were therefore not averaged.

The scale factor was determined from high-order independent-atom-model (IAM) refinements, taking into account only reflections with $\sin\theta/\lambda \geq 0.7$ Å^{-1}. It was fixed in later refinements with improved scattering models. Possible anharmonicity of the atomic displacements was considered by a Gram–Charlier expansion. At the fourth-order level, Sr and Ti atoms have one harmonic and two fourth-order components d_{1111} and d_{1122}, whereas for O atoms there are two harmonic and three fourth-order components d_{1111}, d_{2222} and d_{1122}. With the present high momentum transfer data, reliable probability density functions for each atom are accessible. High-order refinements of the anharmonic components for Sr, Ti and O atoms, separately and together, gave no significant improvements of fit but high correlations with the harmonic parameters. No anharmonic contribution to the temperature factor is thus detected in spite of the high experimental accuracy.

The generalized X-ray scattering-factor model (Stewart, 1976), as implemented in *VALRAY* (Stewart *et al.*, 2000), was used for the crystal electron-density analysis. The radial density functions for the spherically symmetric components were constructed from neutral-atom Hartree–Fock wavefunctions, taken from Clementi & Roetti (1974). The valence shells were assigned as $4s^2 4p^6$ for Sr, $3d^2$ for Ti, and $2s^2 2p^4$ for O atoms. Since the Ti 4*s* and Sr 5*s* valence electrons contribute very little to the scattering, their population cannot be reliably determined and their number was fixed to 2. The difference in scattering power, for example, between Sr^{2+} and the neutral atom for the low-order reflections 100 and 200 amounts to 0.19 and 0.12%, respectively, which is experimentally indistinguishable with an actual counting statistical precision of $\sigma(I)/I = 0.4\%$. A significant difference of 10% occurs only for the unobservable 000 reflection. The Sr and Ti atoms have site symmetry $m\bar{3}m$, where the lowest non-spherical pole is the fourth-order Kubic harmonic, which is a linear combination of the real spherical harmonics y_{40} and y_{44+}. The multipole on the Ti atom was constructed from a 3*d*3*d* atomic orbital self-product. For O atoms, the site symmetry is 4/*mmm* and the

Table 2
Atomic displacement and multipole model parameters.

$U_{\parallel}$(O) is along the Ti—O direction and $U_{\perp}$(O) is in the Sr—O plane. Reliability factors for all observations: $R(F) = 0.0129$, $wR(F^2) = 0.0138$.

Sr	U (Å^2)	0.00577 (1)
	κ	0.976 (3)
	P_{40} (|e| Å^4)	−0.110 (17)
Ti	U (Å^2)	0.00395 (2)
	κ	1 (fixed)
	P_{00} (|e|)	0.218 (45)
	P_{40} (|e| Å^4)	0.56 (11)
O	$U_{\parallel}$ (Å^2)	0.00334 (9)
	$U_{\perp}$ (Å^2)	0.00932 (7)
	κ	0.956 (2)
	P_{00} (|e|)	6.594 (15)
	P_{20} (|e| Å^2)	−0.166 (49)
	P_{40} (|e| Å^4)	0.262 (45)
	P_{44+} (|e| Å^4)	−0.503 (60)

allowed multipoles are $(l,m) = (0,0)$, $(2,0)$, $(4,0)$ and $(4,4+)$. The radial function for the $l = 2$ pole was constructed from a $2p2p$ self-product. For both O and Sr atoms, the $l = 4$ radial function was a single Slater function, $r^4 \exp(-\alpha r)$, with the shell-averaged density values α(O) = 4.50 and α(Sr) = 6.16 bohr^{-1} (Clementi & Roetti, 1974). Charge transfer was introduced between Ti and O atoms, whereas the Sr atom was kept neutral.

In Table 1, the quality of fit is given for the various scattering models. A very large improvement of fit is obtained with a monopole model restricted to charge transfer and valence-shell expansion–contraction. The final atomic displacement and multipole model parameters are reported in Table 2. Note that the reliability factors refer to all observations [$R(F) = 0.0129$, $wR(F^2) = 0.0138$]; corresponding values for the averaged independent data upon completion of refinement are $R(F) = 0.0080$ and $wR(F^2) = 0.0094$. All multipole populations are statistically highly significant. The largest correlation coefficient is 0.77 between U(Sr) and U(Ti). The normalization condition for the aspherical density functions is such that the multipole population coefficients P_{lm} correspond to the local electrostatic moments in ångströms.

As mentioned above, the six strongest low-order reflections have been determined under extinction-free conditions, so that the lowest I_{obs}/I_{kin} ratio was only 0.976 for the full data set. The refined Gaussian mosaic FWHM was 59 (2)″, which is within the experimentally determined range. Consequently, the extinction corrections represent a physically realistic description and not dubious fudge factors.

The six extinction-free structure factors, together with the important 100 reflection, are listed in Table 3. The agreement index, $R(F) = 0.010$, may be considered satisfactory but it is ∼10 times larger than in our previous studies of MnO, CoO and NiO (Jauch & Reehuis, 2004). The reason has to be sought in the different sample characteristics. The mosaic spread of the monoxide specimen was of the order of 10′, which in conjunction with energetic γ-rays ensures almost kinematic scattering conditions. The smaller and somehow anisotropic mosaicity of the $SrTiO_3$ crystal called for a special treatment of extinction effects with the need for an additional sample,

Table 3
Extinction-free low-order structure factors of $SrTiO_3$ at room temperature.

$R(F) = \sum|F_o - F_c|/\sum|F_o| = 0.010$, $R(\sigma) = \sum\sigma(F_o)|/\sum|F_o| = 0.0041$, $R(F;\text{IAM}) = 0.018$.

hkl	$\sin\theta/\lambda$ (Å^{-1})	F_o	F_c
100	0.128	8.79 (2)	8.75
110	0.181	39.88 (18)	39.52
111	0.222	29.54 (19)	29.62
200	0.256	53.29 (11)	53.98
211	0.314	33.12 (13)	32.56
220	0.363	42.66 (14)	42.38
222	0.444	36.18 (23)	35.73

eventually leading to a reduced precision, $R(\sigma) = 0.0041$, as compared to the case of NiO, for example, where $R(\sigma) = 0.0005$ was achieved. One might be tempted to compare Table 3 with the results by Friis *et al.* (2004). These authors have presented experimental static structure factors, without explaining how they managed to find quantities that are not observable. The vibrational and static parts of the structure factor are intimately mixed up in a ternary compound such as $SrTiO_3$, so that the static part cannot be extracted from the measured Bragg intensities but may only be estimated *via* least-squares modelling. Solid-state effects are apparent in Table 3 by noting that the R factor relative to the IAM is 0.018.

4. Form-factor issues

The theoretically computed atomic form factors have to be considered as a possible error component in charge-density modelling. Use of the relativistic Dirac–Fock wavefunctions of Su & Coppens (1998) rather than the non-relativistic Clementi–Roetti wavefunctions results in only very small parameter differences, well within the computed standard uncertainties [except for U(Sr), as explained below], and no improvement of fit. This finding is in contrast to Friis *et al.* (2004) who claim the Hartree–Fock atomic wavefunctions yield poor fits and large κ values.

A better approximation to the exact atomic Rayleigh scattering amplitudes than the ordinary form factor $f(q)$ is the modified relativistic form factor $g(q)$, which takes into account binding effects among the electrons and between electrons and nucleus, and which therefore is no longer the Fourier transform of the radial charge distribution as in the usual form-factor approximation (Kissel *et al.*, 1995). For relativistic electrons, the forward-scattering amplitude is reduced from the classically expected number, $f(0) = Z$, to $g(0) = Z - |E_{tot}|/mc^2$ (E_{tot}: total ground-state binding energy) due to the relativistic increase in mass of the core electrons. A complete tabulation of the total-atom values of $g(q)$ is given by Schaupp *et al.* (1983). In Fig. 1, a comparison of the three types of form factors is presented for the case of strontium. It illustrates that the form factor obtained from non-relativistic wavefunctions comes closer to $g(q)$ than that from relativistic wavefunctions. The disagreement between $g(q)$ and relativistic $f(q)$ increases

Table 4
Characteristics of the bond critical points.

Values of ρ in e Å^{-3}, values of $\nabla^2\rho$ in e Å^{-5}. G, V and G/ρ are given in atomic units.

Bond	$\mathbf{r}_c$	$\rho(\mathbf{r}_c)$	$\nabla^2\rho(\mathbf{r}_c)$	$G(\mathbf{r}_c)$	$V(\mathbf{r}_c)$	$G(\mathbf{r}_c)/\rho(\mathbf{r}_c)$
Ti—O	$\frac{1}{2}$, $\frac{1}{2}$, 0.2486	0.62 (2)	11.73 (3)	0.136 (3)	−0.149 (6)	1.47 (6)
Sr—O	0.2578, 0.2578, 0	0.18 (1)	2.27 (2)	0.023 (5)	−0.022 (10)	0.85 (19)

with higher-Z elements. The reason for this behaviour is to be found in a compensation effect: the increase in scattering amplitude due to relativistic wavefunctions is almost entirely cancelled by the genuine relativistic effect, the reduction due to binding. The substantial discrepancy in the high-order region reveals the failure of the relativistic $f(q)$ to represent the core components properly. Similarly, the shrinkage of the heavy Sr atom arising from the relativistic $f(q)$ is compensated for in turn by a 12σ increase of the displacement parameter. To sum up, non-relativistic form factors are a most appropriate approximation to $g(q)$, which, contrary to widespread belief, recommends their use.

5. Topological characteristics of atomic interactions and atomic charges

The static model electron density was analysed in terms of the atoms-in-molecules (AIM) theory developed by Bader (1990), according to which the interatomic interactions are characterized by the properties of the saddle points (bond critical points $\mathbf{r}_c$) of the electron density between two nuclei, depending on the sign of the associated Laplacian $\nabla^2\rho(\mathbf{r}_c)$. Unshared-electron interaction (ionic bond) is characterized by $\nabla^2\rho(\mathbf{r}_c) \gg 1$ combined with a low value of $\rho(\mathbf{r}_c)$. Further information about the bond properties can be obtained from the local electron energy densities [$G(\mathbf{r}_c)$ = kinetic energy density, $V(\mathbf{r}_c)$ = potential energy density, $H(\mathbf{r}_c) = G(\mathbf{r}_c) + V(\mathbf{r}_c)$ = total energy density] that can be calculated from $\rho(\mathbf{r}_c)$ and $\nabla^2\rho(\mathbf{r}_c)$ using the approximation proposed by Abramov (1997) in combination with the local virial theorem. An ionic bond is revealed by $H(\mathbf{r}_c) \simeq 0$ and a $G(\mathbf{r}_c)/\rho(\mathbf{r}_c)$ ratio greater than unity. The characteristics of the bond critical points are listed in Table 4, and indicate ionic interactions in the Ti—O and Sr—O pairs. The Ti—O bond features closely resemble those found in the ionic prototype NaF, whereas the strength of the Sr—O interaction is much weaker, reflecting the large interatomic distance of 2.76 Å.

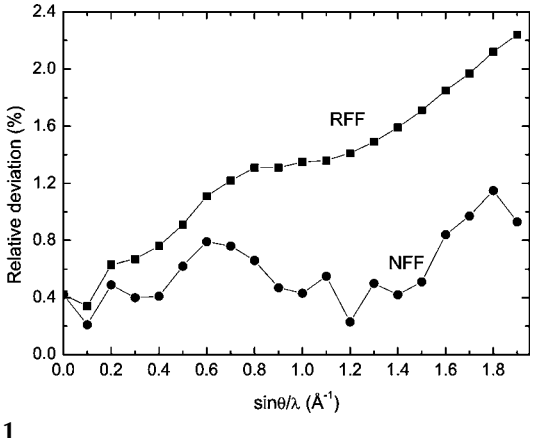

Figure 1
Relative deviation, $(f - g)/f$, of the ordinary non-relativistic (NFF) and relativistic (RFF) form factors from the modified relativistic form factor for strontium.

The atomic charges were determined from the AIM theory by numerical integration of the electron density over the topological atomic basins using the space-partitioning algorithm implemented in *VALRAY* (Flensburg & Madsen, 2000). The charges of the individual basins are found to be q(Sr) = 1.18 |e|, q(Ti) = 3.10 |e| and q(O) = −1.42 |e|; the associated basin volumes are V(Sr) = 16.38, V(Ti) = 6.87 and V(O) = 12.11 Å^3. The integration procedure reproduces the total number of electrons and the unit-cell volume to within 0.03%. Correct partitioning is also indicated by adding up the charges, leading to a neutral entity within the uncertainty. Flensburg & Madsen (2000) find a conservative estimate of the uncertainty in the integrated properties to be less than 5%. With the obtained charges, the Ti and O atoms reach 70–80% of full ionization. The atomic charges characterize the ionicity with the bond strength increasing in proportion to the product of the charges. The integrated charges are thus consistent with the local properties from Table 4, giving further evidence for the ionic nature of bonding in $SrTiO_3$.

6. Discussion and comparison of results

6.1. Thermal vibrations

As mentioned above, there are contradictory results in the literature. From an X-ray diffraction analysis, Abramov *et al.* (1995) report strong anharmonicity for all atoms at T_c + 40 K and for Ti and O atoms at room temperature (RT). A reanalysis of the original data (T_c + 40 K) by Friis *et al.* (2004), however, surprisingly suggests that $SrTiO_3$ is not affected by anharmonicity. According to the present study, $SrTiO_3$ displays purely harmonic behaviour at RT, a result that was also found in our previous γ-ray diffraction study performed at T_c + 5 K and 50 K (Jauch & Palmer, 1999). Our results are in perfect agreement with those by Hutton & Nelmes (1981) [single-crystal neutron diffraction at T_c + 5 K] and Kiat *et al.* (2000) [single-crystal synchrotron and neutron diffraction at RT and T_c + 15 K], which support the absence of anharmonic effects over the whole temperature range.

The O atoms perform strongly anisotropic vibrations corresponding to the libration of the TiO_6 octahedra, which is a precursor of the static tilting below T_c. The $U_{\|}$(O) value, corresponding to motion along the Ti—O bond, is less than that of the heavier Sr and Ti atoms. The displacement parameters from Table 2 are in good agreement with lattice-dynamical calculation: U(Sr) = 0.00647, U(Ti) = 0.00384, $U_{\|}$(O) = 0.00327, $U_{\perp}$(O) = 0.01001 Å^2 (Stirling, 1972). There is also satisfactory agreement with the values from the

synchrotron study by Maslen *et al.* (1995). The harmonic parameters at RT from Abramov *et al.* (1995) are about 40% larger than our values; the same trend is observed for $T_c + 40$ K, where their parameters exceed Stirling's calculated Debye–Waller factors by about 30%. There is a possibility that this problem is related to scan truncation.

6.2. 3*d* valence population on Ti atoms and charge transfer

There are also contradictory results concerning the partial valence charges. In the present study, a much reduced population of the 3*d* subshell for the Ti atoms is found, with a charge transfer of 1.8 e towards the O ligands. In view of the vanishing population, variation of the radial scaling parameter κ(Ti) makes no physical sense and so it was fixed to one. The O atom *L* shell exhibits an expansion of 4.5% in direct space, which is consistent with the change in net charge.

A recent charge-density study of cubic $SrTiO_3$ used combined electron and X-ray diffraction data (Friis *et al.*, 2004). The total number of 3*d* electrons on the Ti atom is reported as large as 2.27 (1), which is further partitioned into the t_{2g} and e_g orbitals. Multipole analysis of calculated structure factors from density functional theory gave an even larger number of 2.73 (1) *d* electrons.

The combined electron/X-ray diffraction method has also been applied to rutile, TiO_2 (Jiang *et al.*, 2003), which has a tetragonal structure with a distorted TiO_6 octahedron. The average Ti—O distance of 1.959 Å is very close to that in $SrTiO_3$. The 3*d* populations on Ti are found to be 2.62 (1) and 2.96 (1) from experimental and band-theory-calculated structure factors, respectively. The population for each of the five non-degenerate *d* orbitals is claimed to be roughly 0.5 e. Any large departure from an empty $3d^0$ outer-shell configuration of the Ti atom is incompatible with the observed magnetic susceptibilities of TiO_2 and $SrTiO_3$, which are temperature-independent (Frederikse & Candela, 1966). According to the above results, these compounds should exhibit Curie paramagnetism with an effective spin magnetic moment of about 3 μ_B. It is worth noting in this connection that subtle magnetic ground-state properties at a subatomic resolution can be extracted from charge-density-derived quantitative information (Jauch, 2004, and references therein).

Interestingly, the O atom monopole parameters for $SrTiO_3$, as reported by Friis *et al.* (2004) and Zhurova & Tsirelson (2002), are equal to the present ones within standard uncertainty. A discrepancy thus occurs essentially only for the metal atom, where, contrary to the authors' assertion, the monopole contains $4s^2$ besides *d*-electron density. Consequently, the calculated 3*d*-orbital occupancies are plainly wrong. The same erroneous confusion was also made in the case of TiO_2.

6.3. Electron density

The static model density, with the Debye–Waller factor omitted, was evaluated in direct space and proved to be positive everywhere in the unit cell. Figs. 2 and 3 show the static deformation densities (aspherical components only). The maximum value of the standard uncertainty in the deformation maps is 0.085 e Å^{-3} at $\frac{1}{2},\frac{1}{2},0.43$.

The pronounced anisotropy and the small maximum/minimum values of the deformation density around the Ti nucleus are consistent with the very light population of the 3*d* subshell. The deformation densities around metal atoms with partially filled *d* shells are at least an order of magnitude larger than in $SrTiO_3$ (*e.g.* Jauch & Reehuis, 2004). The positive lobes on the central Ti atom are directed towards the O ligands, a feature that is in agreement with density functional calculations by Blaha & Schwarz (1994). Conversion of the multipole populations into individual *d*-orbital populations reveals empty t_{2g} orbitals. The remaining *d* electrons occupy only e_g states as illustrated in Figs. 2 and 3.

The experimental deformation densities displayed by Friis *et al.* (2004) and by Zhurova & Tsirelson (2002) show virtually no common features with our maps and can be summarized as follows: (i) the Ti deformations are isotropic, (ii) the Sr valence shell exhibits no asphericity, and (iii) a charge accumulation of around 0.3 e Å^{-3} shows up on the O atom, which is directed towards the Ti atom. Only the theoretical maps by Friis *et al.* (2004), as obtained from density functional theory

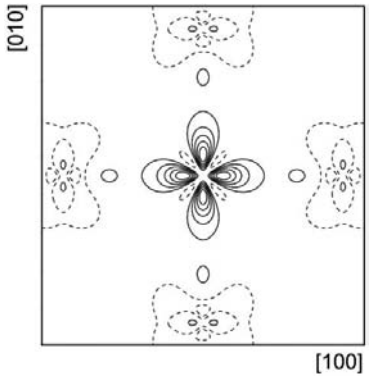

Figure 2
Aspherical contributions to the static model density in the (001) plane. The density range is from −0.19 to 0.42 e Å^{-3}. The Ti atom is located at the centre and the O atoms at the sides of the map. Solid lines represent regions of excessive density, dashed lines depleted regions in steps of 0.07 e Å^{-3}. The zero contour is omitted. The densities are truncated at ±0.35 e Å^{-3}.

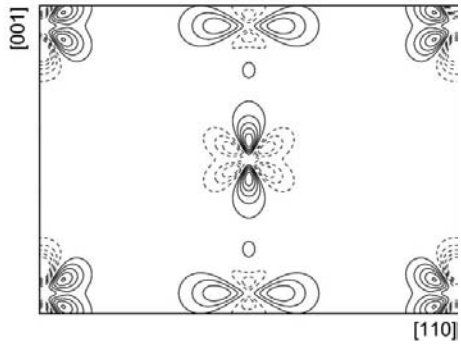

Figure 3
Aspherical contributions to the static model density in the (110) plane. The density range is from −0.53 to 0.41 e Å^{-3}. The Ti atom is located in the centre and the Sr atoms in the corners of the map; the O atoms are above and below the Ti atom. Contours as in Fig. 2.

multipole parameters, reveal a hexadecapole on the Ti atom, which is qualitatively reproduced by our results. The present standard uncertainties for the quadru- and hexadecapole components are significantly smaller than those of previous work as should be expected from the benefits offered by γ radiation. Friis *et al.* (2004) used hexadecapoles on Ti atoms with the population parameter being only 0.3σ. In contrast, our hexadecapole parameter is at the 5σ level.

The charge buildup close to the O atom is not directed towards the Ti atom but rather lies perpendicular to it, and so is a lone-pair peak. Thus an important aspect of the bonding in $SrTiO_3$ is not concentrated along the bond directions. Significant electron deformation is also found quite close to the nucleus of the Sr atom. Its monopole shell exhibits a linear expansion of 2.6%, which should be contrasted with the implausible magnitude of 27% given in Zhurova & Tsirelson (2002).

6.4. Bonding state

The conclusion by Friis *et al.* (2004) and Zhurova & Tsirelson (2002) that the Ti—O interaction is polar covalent is not supported by the values of the topological criteria obtained in the present study. Their conclusion is based on the so-called bonding peak on the O atom, which is interpreted as a covalent component. The value of $H(\mathbf{r}_c)$ for the Ti—O bond obtained by Zhurova & Tsirelson (2002) is significantly negative and has been regarded as an additional signature of covalency. The corresponding result from Table 4, however, turns out to be virtually zero, $H(\mathbf{r}_c) = -0.013$ (6) a.u., which suggests an ionic bonding situation.

Synchrotron X-ray powder diffraction data, up to $\sin\theta/\lambda = 0.88$ Å^{-1} at RT, were employed in an attempt to gain insight into the charge density of $SrTiO_3$ by means of a maximum-entropy analysis (Ikeda *et al.*, 1998). The MaxEnt reconstruction of the total dynamic density (*i.e.* thermal motion included) shows an elongation of the Ti-atom density at the 1 e Å^{-3} level towards the O atoms, which was interpreted as a covalent bonding ridge. In Fig. 4, the total static electron density (*i.e.* no thermal motion) is mapped directly from the γ-ray-derived multipole parameters on the same scale as in Ikeda *et al.* (1998). The perfectly spherical shape of Ti is clearly visualized as well as the asphericity of the O atom due to the lone-pair charge pile up. From single-crystal experience, it is known that MaxEnt features in low-density regions, below about 2 e Å^{-3}, tend to be contaminated with spurious artifacts because of the large dynamic range of the total density (Jauch & Palmer, 1993). This problem is aggravated in the powder diffraction case with its inherent inferior quality of the data. As a consequence, MaxEnt indeed fails to recover the strong anisotropy of thermal vibration of the O atom.

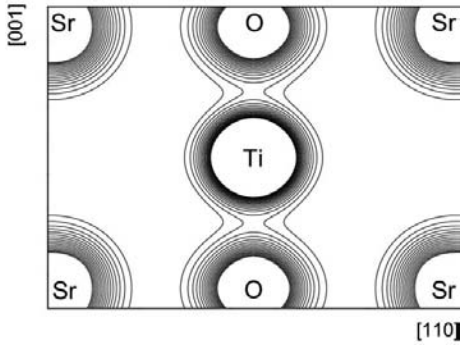

Figure 4
Total static model density in the (110) plane (same part as in Fig. 3). The density range is from 0.4 to 3.4 e Å^{-3} in steps of 0.2 e Å^{-3}.

7. Concluding remarks

An extended set of high-quality structure factors, achieved by the use of 316.5 keV γ radiation, has resulted in the most reliable electron distribution of $SrTiO_3$ available to date. The extinction problem has been resolved by the extended-face flat crystal method. Important findings of the present study include the following: (i) the thermal displacement parameters are in good agreement with lattice dynamical calculations as well as with neutron diffraction results and additionally show that anharmonic motion is negligible for all atoms; (ii) the Ti—O bond is identified as strongly ionic whereas the Sr—O bond has a weaker ionic character; (iii) the population of the 3*d* subshell for the Ti atom is found close to zero; (iv) there is significant deformation density on the Sr atom. Application of γ radiation thus has permitted new insights into the electronic structure of an important material.

We are grateful to Dr H.-J. Bleif for helpful discussions and support and to Dr H. O. Sørensen for evaluation of the AIM charges.

References

Abramov, Yu. A. (1997). *Acta Cryst.* A**53**, 264–272.
Abramov, Yu. A., Tsirelson, V. G., Zavodnik, V. E., Ivanov, S. A. & Brown, I. D. (1995). *Acta Cryst.* B**51**, 942–951.
Bader, R. F. W. (1990). *Atoms in Molecules: a Quantum Theory.* Oxford: Clarendon Press.
Becker, P. J. & Coppens, P. (1975). *Acta Cryst.* A**31**, 417–425.
Bell, R. O. & Rupprecht, G. (1963). *Phys. Rev.* **129**, 90–97.
Blaha, P. & Schwarz, K. (1994). *Z. Kristallogr. Suppl.* **8**, 542.
Clementi, E. & Roetti, C. (1974). *At. Data Nucl. Data Tables*, **14**, 177–478.
Flensburg, C. & Madsen, D. (2000). *Acta Cryst.* A**56**, 24–28.
Frederikse, H. P. R. & Candela, G. A. (1966). *Phys. Rev.* **147**, 583–584.
Friis, J., Jiang, B., Spence, J., Marthinsen, K. & Holmestad, R. (2004). *Acta Cryst.* A**60**, 402–408.
Hall, S. R., King, G. S. D. & Stewart, J. M. (1995). *Xtal3.4 User's Manual*, University of Western Australia, Australia.
Hubbel, J. H. (1982). *Int. J. Appl. Radiat. Isot.* **33**, 1269–1290.
Hutton, J. & Nelmes, R. J. (1981). *J. Phys. C Solid State Phys.* **14**, 1713–1736.
Ikeda, T., Kobayashi, T., Takata, M., Takayama, T. & Sakata, M. (1998). *Solid State Ionics*, **108**, 151–157.
Jauch, W. (2004). *Acta Cryst.* A**60**, 397–401.
Jauch, W. & Palmer, A. (1993). *Acta Cryst.* A**49**, 590–591.
Jauch, W. & Palmer, A. (1999). *Phys. Rev. B*, **60**, 2961–2963.
Jauch, W. & Reehuis, M. (2004). *Phys. Rev. B*, **70**, 195121-1–8.
Jiang, J., Zuo, J. M., O'Keefe, M. & Spence, J. C. H. (2003). *Acta Cryst.* A**59**, 341–350.

Kiat, J.-M., Baldinozzi, G., Dunlop, M., Malibert, C., Dkhil, B., Ménoret, C., Masson, O. & Fernandez-Diaz, M.-T. (2000). *J. Phys. Condens. Matter*, **12**, 8411–8425.
Kissel, L., Zhou, B., Roy, S. C., Gupta, S. K. S. & Pratt, R. H. (1995). *Acta Cryst.* A**51**, 271–288.
Maslen, E. N., Spadaccini, N., Ito, T., Marumo, F. & Satow, Y. (1995). *Acta Cryst.* B**51**, 939–942.
Okazaki, A. & Kawaminami, M. (1973). *Mater. Res. Bull.* **8**, 545–550.
Schaupp, D., Schumacher, M., Smend, F. & Rullhusen, P. (1983). *J. Phys. Chem. Ref. Data*, **12**, 467–512.
Skelton, E. F. & Katz, J. L. (1969). *Acta Cryst.* A**25**, 319–329.
Spackman, M. A. (1998). *Ann. Rep. Prog. Chem. Sect. C, Phys. Chem.* **94**, 177–207.
Stewart, R. F. (1976). *Acta Cryst.* A**32**, 565–574.
Stewart, R. F., Spackman, M. A. & Flensburg, C. (2000). *VALRAY User's Manual.* Carnegie-Mellon University, Pittsburgh, PA, USA, and University of Copenhagen, Denmark.
Stirling, W. G. (1972). *J. Phys. C Solid State Phys.* **5**, 2711–2730.
Su, Z. & Coppens, P. (1998). *Acta Cryst.* A**54**, 646–652.
Zhurova, E. A. & Tsirelson, V. G. (2002). *Acta Cryst.* B**58**, 567–575.